VLT/NACO infrared adaptive optics images of small scale structures in OMC1

F Lacombe, E Gendron, D Rouan, Y Clénet, D Field, L. Lemaire, M Gustafsson, A.-M Lagrange, D Mouillet, G Rousset, et al.

A&A 417, L5–L9 (2004)
DOI: 10.1051/0004-6361:20040030

Astronomy & Astrophysics

VLT/NACO infrared adaptive optics images of small scale structures in OMC1⋆

F. Lacombe[1], E. Gendron[1], D. Rouan[1], Y. Clénet[1], D. Field[2], J. L. Lemaire[3,4], M. Gustafsson[2], A.-M. Lagrange[5], D. Mouillet[5], G. Rousset[6], T. Fusco[6], L. Rousset-Rouvière[6], B. Servan[7,†], C. Marlot[1], and P. Feautrier[5]

[1] LESIA – Observatoire de Paris-Meudon, UMR 8109 CNRS, 92195 Meudon, France
e-mail: francois.lacombe@obspm.fr; daniel.rouan@obspm.fr
[2] Institute for Physics and Astronomy, Århus University, 8000 Århus C, Denmark
e-mail: dfield@phys.au.dk
[3] LERMA – Observatoire de Paris-Meudon, UMR 8112 CNRS, 92195 Meudon, France
e-mail: jean-louis.lemaire@obspm.fr
[4] Université de Cergy-Pontoise, 95031 Cergy Cedex, France
[5] LAOG – Observatoire de Grenoble, UMR 5571 CNRS, 38041, Grenoble, France
[6] ONERA – DOTA, 92322 Châtillon, France
[7] GEPI – Observatoire de Paris-Meudon, UMR 8111 CNRS, 92195 Meudon, France

Received 18 March 2003 / Accepted 3 July 2003

Abstract. Near-infrared observations of line emission from excited H_2 and in the continuum are reported in the direction of the Orion molecular cloud OMC1, using the European Southern Observatory Very Large Telescope UT4, equipped with the NAOS adaptive optics system on the CONICA infrared array camera. Spatial resolution has been achieved at close to the diffraction limit of the telescope (0.08″–0.12″) and images show a wealth of morphological detail. Structure is not fractal but shows two preferred scale sizes of 2.″ (1100 AU) and 1.2″ (540 AU), where the larger scale may be associated with star formation.

Key words. ISM: individual objects: OMC1 – ISM: circumstellar matter – ISM: kinematics and dynamics – ISM: molecules – infrared: ISM

1. Introduction

Near infrared (NIR) observations, performed with the European Southern Observatory Very Large Telescope (ESO-VLT), are described which provide high spatial resolution images of the Orion Molecular Cloud (OMC1; distance 460 pc, Bally et al. 2000). Data are presented in the $v = 1{-}0$ S(1) line of H_2 at 2.121 μm and in continuum emission at nearby wavelengths. Earlier NIR imaging of this zone may be found for example in Allen & Burton (1993), Brand (1995), Schild et al. (1997), McCaughrean & MacLow (1997), Chrysostomou et al. (1997), Chen et al. (1998), Stolovy et al. (1998), Schultz et al. (1998), Lee & Burton (1999), Tedds et al. (1999), Salas et al. (1999), Vannier et al. (2001, V2001), Gustafsson et al. (2003, G2003), Kristensen et al. (2003, K2003). The nature of the Orion Nebula Cluster, in which OMC1 is embedded, is reviewed in O'Dell (2001) and Ferland (2001). As discussed there, OMC1 consists of dense fragments of gas and dust, in part situated within the HII region, which itself constitutes the visible Orion Nebula. The interest in OMC1 and the surrounding zone stems from widespread ongoing star-formation in this region (e.g. Luhman et al. 2000), exemplified through the presence of many protostars, outflows and larger scale flows, for example the explosive Becklin-Neugebauer-IRc2 complex (BN-IRc2) in OMC1 (see O'Dell 2001; Allen & Burton 1993; Doi et al. 2002; O'Dell & Doi 2003).

In the present work we use the VLT-UT4 with NACO, an association of the new adaptive optics system NAOS (Nasmyth Adaptive Optics System) and the CONICA (COudé Near IR Camera) infrared array camera (Lenzen et al. 1998; Rousset et al. 2000; Brandner et al. 2002). This yields, in part of the full image, a spatial resolution two to three times higher than that achieved previously with the HST (Stolovy et al. 1998; Schultz et al. 1998) or with 4 m-class telescopes using adaptive optics e.g. the Canada-France-Hawaii Telescope (V2001; G2003; K2003).

Our present data allow us to address the issue of the scale sizes of clumps of excited H_2 in OMC1 with significantly greater precision and over a region within OMC1 roughly an order of magnitude larger in the plane of the sky than in earlier work (V2001). In this connection, V2001 showed that

Send offprint requests to: D. Rouan,
e-mail: daniel.rouan@obspm.fr

⋆ Based on observations collected at the ESO/Paranal YEPUN telescope, Proposal 70.C-0315.

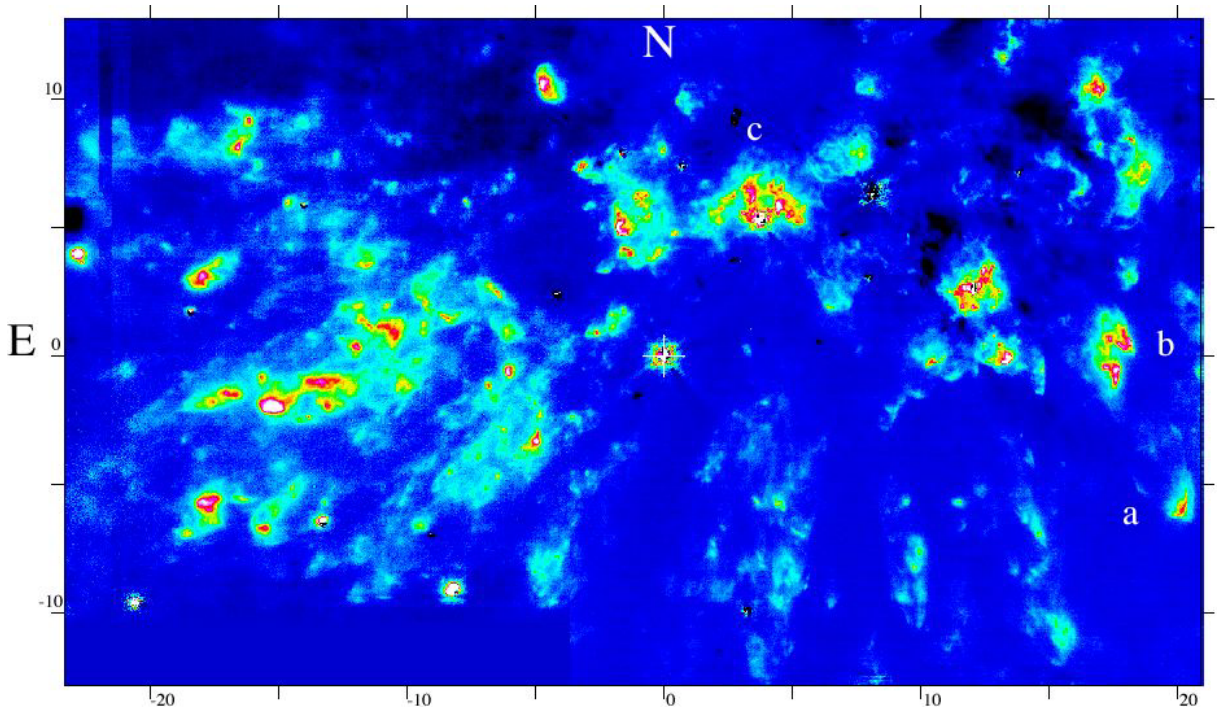

Fig. 1. H_2 emission in the 1−0 S(1) line at 2.121 μm, with continuum emission subtracted. Image size: 44.5″ × 26″. The cross indicates the position of the star TCC016 ($05^h35^m14^s.91$, $-05°22'39''.31$ (J2000)) and a,b,c identify objects shown in more detail in subsequents. The SE and ESE frames, referred to in the text, are respectively the regions to the west and to the east of TCC0016.

H_2 emitting regions did not exhibit fractal structure but showed a preferred scale of between 3 and 4×10^{-3} pc. Here we corroborate this finding and also identify a second preferred scale size of about half this value, in a neighbouring region of OMC1, to the west of that studied in V2001.

2. Observations and data reduction

Observations of OMC1 were performed with the VLT UT4 during guaranteed NACO time on the 21st of November 2002, for about 4.5 h in total. The seeing was variable during this night ranging from 0.65″ to 1.13″. Two regions have been observed located south-east (SE frame) and east-south-east (ESE frame) from BN and IRc2, with the star TCC016 (Fig. 1) common to both frames. The IR wavefront sensor (WFS) was used for the SE frame using BN ($m_K \sim 8$) as the adaptive optics (AO) reference star. The average seeing was ∼0.85″ and the resulting *FWHM* of the PSF measured on several stars in the SE field was ∼0.08″. The ESE frame was recorded using the visible WFS locked on the star TCC016 ($m_V \sim 14$) which, combined with an average seeing of ∼1.03″, led to a measured *FWHM* of the PSF of ∼0.12″. The Strehl ratio was clearly higher in the SE frame, giving nearly full correction by the AO system to the diffraction limit of ∼0.06″. Using camera mode S27, the field of view was 27.6″ × 27.6″ and the pixel scale was 0.027″, a size sufficient to satisfy the Nyquist sampling criterion. 0.027″ corresponds to 12 AU at the distance of Orion.

Filters were used at 2.121 ± 0.011 μm (NB212), which contains the H_2 S(1) $v = 1-0$ line, IB224, at 2.24 ± 0.03 μm and IB227 at 2.27 ± 0.03 μm. IB224 includes the H_2 1−0 S(0) line at 2.223 μm and the H_2 2−1 S(1) line at 2.247 μm, as well as [FeII] lines at 2.218 and 2.242 μm. IB227 includes the H_2 2−1 S(1) line and the [FeII] line at 2.242 μm. The AutoJitter mode was used, that is, at each exposure, the telescope moves according to a random pattern in a 6″ × 6″ box. Cross-correlation was used to recenter the images at ≈0.15 pixel. For the ESE frame, an empty background sky has been recorded for the purpose of sky subtraction. For the other less crowded SE frame, the background sky has been created by performing a median filtering of the set of 32 randomly jittered individual frames. The total exposure time on object for each filter was 800 s for the SE frame and 1500 s for the ESE frame, with exposures of 10 s for each data acquisition.

To obtain an image in the H_2 $v = 1-0$ S(1) line, the IB244 continuum image was subtracted from the NB212 image after division by a factor of 2.5 as derived from measuring fluxes of a dozen of stars in both filters.The resulting image is shown in Fig. 1. The contribution of $v = 1-0$ S(0) and $v = 2-1$ S(1) in IB224, known to be small from spectroscopy, was ignored in image processing. By subtraction of the image in the IB227 filter from that in the IB224, using a conversion factor obtained as before from stellar fluxes, it was possible to obtain an image in H_2 S(0) $v = 1-0$, less the weaker emission in $v = 2-1$ S(1), but plus the very weak FeII line at 2.218 μm. The image in $v = 1-0$ S(0) shows essentially the same structure as that in Fig. 1, but is 4 to 5 times weaker. An example of data in $v = 1-0$ S(0) is shown in Fig. 3c.

Strong continuum emission is seen for example in the northern part of the ESE region and is shown in Fig. 2, which displays emission in the IB227 filter. Data in Fig. 2 also include weak emission from $v = 2-1$ S(1) and [Fe II]

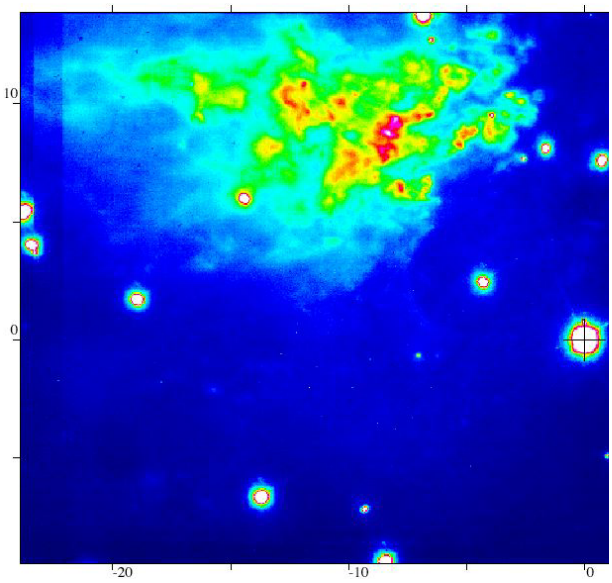

Fig. 2. Continuum emission at 2.27 ± 0.03 μm in the ESE field. Image size: 27.6″ × 23.4″. The position of TCC0016 is marked with a cross.

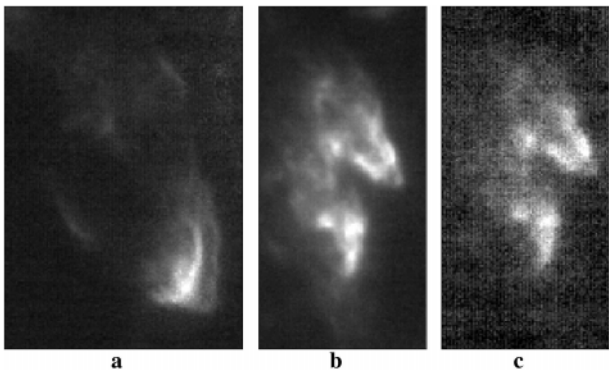

Fig. 3. a) A detailed view (3.5″ × 5.0″) of object a (see Fig. 1) in v = 1−0 S(1) H_2 emission at 2.121 μm. **b)** of object b (2.5″ × 5.0″) in the same line. **c)** Detail (2.5″ × 5.0″) of object b in the 1−0 S(0) H_2 emission line at 2.22 μm.

(Schultz et al. 1999). Continuum emission is also seen at this position in the data of Schultz et al. (1999).

3. Discussion of results

3.1. Origin of the NIR emission

H_2 emission in OMC1 arises from heating in J-type and C-type (magnetic) shocks (e.g. Draine et al. 1983; Pineau des Forêts et al. 1988; Smith & Brand 1990; Kaufman & Neufeld 1996a,b; Timmerman 1998; Wilgenbus et al. 2000; V2001; Le Bourlot et al. 2002; K2003; G2003) and from photon excitation in photodissociation regions (PDRs) e.g. Störzer & Hollenbach (1999), Sternberg & Dalgarno (1989), Black & van Dishoeck (1987), Black & Dalgarno (1976).

Shocks in the region observed arise from one or more large-scale outflows, thought to originate from the BN-IRc2 region (O'Dell & Doi 2003; Doi et al. 2002; O'Dell 2001, and references therein). Shocks in the zone observed may also arise from

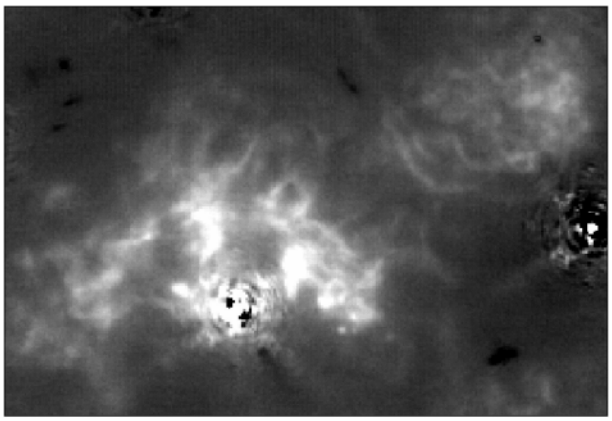

Fig. 4. A detailed view of object c (see Fig. 1) in v = 1−0 S(1) H_2 emission at 2.121 μm. Image size: 7.5″ × 5.0″.

local outflows associated with protostars buried within emitting clumps of gas (G2003).

PDRs are generated through the action of the Trapezium stars, to the south of the present region, of which the dominant contributor is θ^1Ori C. This star generates far-UV radiation fields of $>10^5$ times the standard interstellar field over much of OMC1, and is in addition the chief contributor to the HII region in which dense clumps in OMC1 may be bathed. The BN object is a young and massive B-star (Gezari et al. 1998) and may also provide a source for PDR excitation.

The relative importance of PDR and shock excitation in the strongest emitting regions has been discussed in detail in K2003. The conclusion is that in the subset of clumps studied in that work, which are those to the east of TCC016 in the ESE image, C-type shocks are the major contributor to H_2 excitation. However, towards the fringes of bright clumps, J-type shock and PDR excitation by θ^1Ori C take the place of C-type shock excitation, with shock and PDR excitation contributing roughly equally. In all cases of very bright emission, both in the cores of clumps and at their fringes, the densities are high, exceeding several times 10^7 to $>10^8$ cm^{-3}. Excited gas, formed in numerous, individually unresolved shocks, rapidly accumulates into cold compressed zones and excited H_2 is the very rapid progenitor of cold dense gas. Thus the structure of excited H_2, discussed in Sect. 3.2 below, provides a measure of the structure of cold H_2 clumps, where the latter is the gas from which stars will ultimately form.

In other regions, which are presumably less dense, the correspondingly larger shock structure appears to be clearly resolved in H_2 emission. This is illustrated by data in Figs. 3–5. Numerous objects in these figures resemble bow shocks. The general appearance of this figure suggests that the region may be permeated by supersonic turbulence giving rise to shocks in all directions. The emission may also in part be due to complex density structure with PDR excitation. At all events, our NACO data allow us to specify the width of the filamentary regions containing excited gas. For example in Fig. 5, showing the western part of object c (Fig. 4) and of object a (Fig. 3) in greater detail, widths of some filaments appear marginally resolved. If these scales of ≈40–50 AU are shock widths, these data provide important constraints on shock

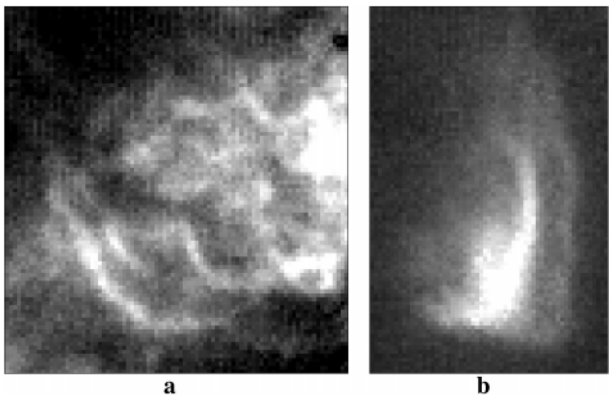

Fig. 5. a) Detail (1.56″ × 2.40″) of the NW part of Fig. 4 and **b)** of Fig. 3a (2.24″ × 2.40″) showing narrow filamentary structure.

models (Le Bourlot et al. 2002; Wilgenbus et al. 2000), in which parameters of density, magnetic field and shock speed determine the shock width. If the features are PDRs, the widths of structures are again valuable parameters, providing a good indicator of the gas density (K2003; Lemaire et al. 1996; Sternberg & Dalgarno 1989). An additional constraint to shock or PDR models is provided by data for the $v = 1{-}0$ S(0) line, see Fig. 3c. In future work, we will pursue modeling of these regions, including constraints arising from absolute brightness in the H_2 emission lines.

The origin of the diffuse continuum emission (plus [FeII] and some weak H_2 emission – see above), for example in Fig. 2, is most likely reflected light from dust. In this connection, there is little shock excitation where strong continuum emission is observed, as a comparison of Figs. 1 and 2 reveals. Thus little mechanical energy is being injected into this zone. Emission could arise from far-UV photon heating of very small dust particles, as for example in NGC7023 (Lemaire et al. 1996), with θ^1Ori C and BN as sources in the present case. There is however strong circular polarization in the *K*-band continuum in the zone shown in Fig. 2 (Chrysostomou et al. 2000). Those authors ascribed the origin of circular polarization to scattering from oblate grains oriented in magnetic fields. There is in fact striking spatial correlation, lying within the observational resolution of the circular polarization data, between the regions of strong circular polarization reported in Chrysostomou et al. (2000) and the continuum emission seen in Fig. 2 and at other positions throughout the SE and ESE images. If we include the linear polarization data of Geng (1993), then effectively in all regions in which continuum emission is observed, either circular or linear polarized *K*-band radiation may be found. This lends strong support to the hypothesis that the observed diffuse emission in the continuum is due to scattering from dust. According to Chrysostomou et al. (2000), the source of illumination is not the Trapezium stars, but is intrinsic to OMC1 through some unidentified source.

Weak [FeII] emission is present for example in the region shown in Fig. 2 (Schultz et al. 1999) and most likely arises from photoionization and excitation by θ^1Ori C in the HII plasma as suggested in Schultz et al. (1999). In this model, [FeII] emission is projected over the *K*-band continuum emission discussed above.

3.2. Analysis of small scale structures

V2001 gave the first clear indication that the size distribution of hot H_2 clumps in Orion was not fractal, using data for a small region of OMC1, 12.8″ × 12.8″, in the southern part of the ESE region of the present work. In order to analyze the global nature of small scale structure, V2001 used area-perimeter, Fourier, brightness histogram (Blitz & Williams 1997) and direct measurement analyses. All techniques revealed that structure observed in $v = 1{-}0$ S(1) H_2 emission was not fractal and all yielded the same preferred scale size. Here we choose the brightness histogram method for its simplicity and ease of interpretation.

In brief, this method involves counting in the original image the number of pixels $N(B_n)$, binned into some small normalized brightness range, as a function of the pixel normalized brightness, B_n. B_n is defined as the value of brightness in any pixel divided by the value in the brightest pixel in the image. The resolution of the image is then degraded by boxcar averaging over some chosen number of pixels on a square and a new set of $N(B_n)$ and B_n calculated. This process is repeated, successively degrading the resolution of the image. Plots of $N(B_n)/N_{\rm Tot}$ vs. B_n, where $N_{\rm Tot}$ is the total number of pixels, yield a set of curves which remain unchanged for an image with no preferred scale, that is, a fractal image, as the resolution of the image is degraded. By contrast, for an image with a preferred scale, such plots should change in form as the resolution is degraded to the point at which any preferred scale has been washed out. Beyond this critical smoothing, the form of such plots should remain constant, mimicking a fractal. The amplitude of the critical smoothing is a direct measure of the preferred range of scale in the image. In all cases stars were masked out in the images before the brightness histogram analysis was performed.

A brightness histogram analysis for the ESE image in H_2 is shown in Fig. 6. We estimate that the preferred scale for regions of excited H_2 is encountered when averaging is performed over 90 ± 5 × 90 ± 5 pixels, that is, at a scale of 2.4 ± 0.14″ (1075 AU). An exactly similar analysis on the SE region, that is, to the west of TCC016 in Fig. 1, yields a preferred scale of 1.2 ± 0.14″ (540 AU). If we choose a region which samples approximately equally both the ESE and SE regions and perform a brightness histogram analysis, we encounter two scales present together, of 2.4″ and 1.2″. We conclude therefore that the ESE region contains clumps of material of about twice the scale of the material in the SE region, with a well-defined demarcation between them. The same analysis has been applied to the image in the continuum, shown in Fig. 2. This yields a scale of 2.15 ± 0.28″. This indicates that dust, and by implication, cold unexcited gas in this region is clumped on the same scale as in the shocked southern region in ESE. The scale size, if one is present, of continuum emission in the SE region could not be determined using the technique described here, but is larger than 2.7 arcsec. Data covering a

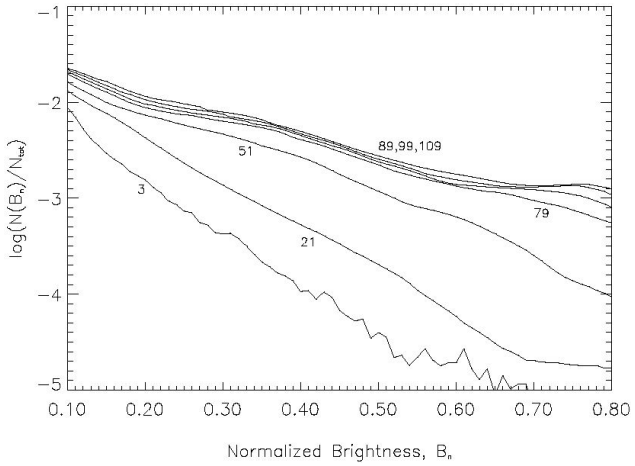

Fig. 6. Brightness histogram analysis of the H_2 $v = 1{-}0$ S(1) emission at 2.121 μm in the ESE region. Figures besides the curves shown represent the number of pixels on the square over which the data have been spatially averaged.

more extensive field in OMC1 may yield information in the future.

The scale-size identified in V2001, for a subset of the ESE region, was $2.0 \pm 0.1''$, in substantial agreement with the present work. As described in detail in V2001, the brightness of emission of H_2 may be used in conjunction with C-type magnetic shock models to show that in bright emissions regions the dense gas, swept up by the shock, will achieve densities of several times 10^7 cm^{-3}, as the post-shock gas cools to 10 K. Related data for the $v = 2{-}1$ S(1) emission line, discussed in K2003, show that densities may be locally even higher, exceeding 10^8 cm^{-3} in some regions. Our present estimates of clump size add weight to the conclusion in V2001, based upon Jeans length considerations, that sufficient gas has accumulated through shock induced compression to form gravitationally unstable clumps which are potential sites of star formation, in the ESE region. This shock-induced mechanism would not appear to be presently effective in hastening star-formation in the SE region, since we find that the clump masses are typically an order of magnitude smaller than in ESE and comprise no more than 0.01 to 0.02 $M_\odot$ if we assume densities of $<10^8$ cm^{-3} given the observed size of $1.2''$. In connection with the interpretation of our data, results in G2003 appear to show that protostars may already have formed in certain of the zones very bright in H_2 emission. In some regions we may therefore be observing the aftermath of very recent star formation rather than the period just prior to gravitational collapse.

Acknowledgements. DF and MG acknowledge the support of the Aarhus Centre for Atomic Physics, funded by the Danish Basic Research Foundation. JLL and DR acknowledge support of the french PCMI program, funded by CNRS.

References

Allen, D. A., & Burton, M. G. 1993, Nature, 363, 54
Bally, J., O'Dell, C. R., & McCaughrean, M. J. 2000, AJ, 119, 2919
Black, J. H., & Dalgarno, A. 1976, ApJ, 203, 132
Black, J. H., & van Dishoeck, E. F. 1987, ApJ, 322, 412
Blitz, L., & Williams, J. P. 1997, ApJ, 488, L145
Brand, P. W. J. L. 1995, ApJSS, 233, 27
Brandner, W., Rousset, G., Lenzen, R., et al. 2002, The ESO Messenger, 107, 1
Chen, H., Bally, J., O'Dell, C. R., et al. 1998, ApJ, 492, L173
Chrysostomou, A., Burton, M. G., Axon, D. J., et al. 1997, MNRAS, 289, 605
Chrysostomou, A., Glendhill, T. M., Ménard, F., et al. 2000, MNRAS, 312, 103
Draine, B. T., Roberge, W. G., & Dalgarno, A. 1983, ApJ, 264, 485
Ferland, G. J. 2001, PASP, 113, 41
Geng, F. 1993, Ph.D. Thesis, University of Tokyo, Data are shown in Chrysostomou et al. (2000)
Gezari, D. Y., Backman, D. E., & Werner, M. W. 1998, ApJ, 509, 283
Gustafsson, M., Kristensen, L. E., Clénet, Y., et al. 2003, A&A, 411, 437
Kaufman, M. J., & Neufeld, D. A. 1996a, ApJ, 456, 250
Kaufman, M. J., & Neufeld, D. A. 1996b, ApJ, 456, 611
Kristensen, L., Gustafsson, M., Field, D., et al. 2003, A&A, 412, 727
Le Bourlot, J., Pineau des Forêts, G., Flower, D. R., & Cabrit, S. 2002, MNRAS, 332, 985
Lee, J.-K., & Burton, M. G. 2000, MNRAS, 315, 11
Lemaire, J. L., Field, D., Gerin, M., et al. 1996, A&A, 308, 895
Lenzen, R., Hofmann, R., Bizenberger, P., et al. 1998, Proc. SPIE, 3354, 606
McCaughrean, M. J., & MacLow, M. M. 1997, AJ, 113, 391
O'Dell, C. R. 2001, ARA&A, 39, 99
O'Dell, C. R., & Doi, T. 2003, AJ, 125, 277
Pineau des Forêts, G., Flower, D. R., & Dalgarno, A. 1988, MNRAS, 235, 621
Rousset, G., Lacombe, F., Puget, P., et al. 2000, Proc. SPIE, 4007, 72
Salas, L., Rosado, M., Cruz-Gonzales, I., et al. 1999, ApJ, 511, 822
Schild, H., Miller, S., & Tennyson, J. 1997, A&A, 318, 608
Schultz, A. S. B., Colgan, S. W. J., Erickson, E. F., et al. 1999, ApJ, 511, 282
Smith, M. D., & Brand, P. W. J. L. 1990, MNRAS, 242, 495
Sternberg, A., & Dalgarno, A. 1989, ApJ, 338, 197
Stolovy, S. R., Burton, M. G., Erikson, E., et al. 1998, ApJ, 492, L151
Störzer, H., & Hollenbach, D. J. 1999, ApJ, 515, 669
Tedds, J. A., Brand, P. W. J. L., & Burton, M. G. 1999, MNRAS, 307, 337
Timmerman, R. 1998, ApJ, 498, 246
Vannier, L., Lemaire, J. L., Field, D., et al. 2001, A&A, 366, 651
Wilgenbus, D., Cabrit, S., Pineau des Forêts, G., & Flower, D. R. 2000, A&A, 356, 1010